Electronic Supplementary Material (ESI) for Journal of Materials Chemistry C.

Supporting Information For "Long-Lived Highly Emissive MOFs as Potential Candidates for Multiphotonic Applications"

Mario Gutiérrez, Cristina Martín, Johan Hofkens, and Jin-Chong Tan**

[1]Multifunctional Materials & Composites (MMC) Laboratory, Department of Engineering Science, University of Oxford, Parks Road, Oxford OX1 3PJ, United Kingdom.

[2]Chem&Tech - Molecular Imaging and Photonics, KU Leuven, Celestijnenlaan 200F, B-3001 Leuven, Belgium.

[3]Unidad nanoCRIB. Centro Regional de Investigaciones Biomédicas, Albacete-02071, Spain.

***Corresponding authors**

E-mail: jin-chong.tan@eng.ox.ac.uk

E-mail: cristina.malvarez@uclm.es

Index

1. Experimental Techniques 2
2. Synthesis of Pb-BDC MOFs 3
3. Structural, Morphological, Chemical & Thermogravimetric Characterization 3-6
4. Long-Lived Time-Resolved Characterization 7
5. Chemical Detection 8-9
6. Thermochromism 10
7. LEDs 11-12
8. References 13

1. Experimental Techniques

Powder X-ray diffraction (PXRD): Powder X-ray diffraction experiments were carried out in a Rigaku MiniFlex X-ray diffractometer with a Cu Kα source (1.541 Å). The diffraction data were collected using 0.01° step size, 1° min^{-1} scan rate and at 2θ angle ranging from 2° to 32°.

Scanning electron microscopy (SEM): Focus ion beam scanning electron microscopy (FIB-SEM) were obtained using the Tescan LYRA3 XM FIB-SEM instrument with an electron and focus ion beam gun. Micrographs were attained in secondary electron imaging mode under high vacuum with an accelerating voltage of 10 keV.

Fourier transform infrared spectroscopy (FTIR): FTIR measurements were performed on a Bruker IFS 66v/S spectrometer. Thin transparent wafers of KBr mixed with 1 wt% of sample were prepared and dried at 60°C and 80°C

Thermogravimetric analysis (TGA): TGA of the samples was performed using a TA Instruments Q500 thermogravimetric analyser. The samples were treated under an oxygen flow with a linear heating ramp of 10°C/min to 650 °C. TA Universal Analysis software was used for post-measurement data handling.

Photoluminiscence Experiments: Steady-state fluorescence spectra and luminescence quantum yields were recorded using the FS-5 spectrofluorometer (Edinburgh Instruments) equipped with different modules for each specific experiment (i.e. integrating sphere for quantum yield, heated sample module to measure the emission of powders at different temperatures and a standard solid holder for powder experiments).

2. Synthesis of Pb-BDC MOFs

The Pb-BDC MOFs were synthesized following the methodology previously described for silver-based OX-2 MOFs [1], with minor modifications.

Pb-BDC/H_2O: A solution of 3.0 mmol of terephthalic acid (BDC) was deprotonated through the addition of double amount, 6.0 mmol of triethylamine (NEt_3), in 20 mL of water. Simultaneously, 3.0 mmol of $PbNO_3$ were dissolved in 20 mL of water by sonicating the mixture. After that, the latter solution was added to the former one under stirring and a white suspension was promptly formed. This suspension was stirred for 2 hours, and then, the white solid sample was washed several times with water, collected by centrifugation (8000 rpm) and dried at 80 °C for 2 h. This procedure gave 1 g of white Pb-BDC/H_2O powder.

Pb-BDC/DMF: This MOF was synthesized similarly to the above one. A solution of 6.0 mmol of terephthalic acid and 12.0 mmol of triethylamine (NEt_3) in 20 mL of N,N-dimethylformamide (DMF) was prepared. In parallel, 6.0 mmol of $PbNO_3$ were dissolved in 20 mL of DMF by sonicating the mixture. Both solutions were mixed under stirring and a white suspension was promptly formed. The suspension was then stirred for 2 hours, and the obtained white powder was washed 3 times with DMF and collected by centrifugation (8000 rpm). The sample was carefully dried at 80 °C for 1 h. This procedure gave ~2 g of white Pb-BDC/DMF powder.

3. Structural, Morphological & Chemical Characterization

The Pb-BDC MOFs were structurally, morphologically and chemically characterized by a combination of powder X-ray diffraction (PXRD), scanning electron microscopic (SEM), atomic force microscopic (AFM), Fourier transformed infrared spectroscopic (FTIR) and thermogravimetric techniques.

Structural Characterization: The PXRD diffractograms of Pb-BDC/H_2O and Pb-BDC/DMF are shown in Figure S1 and compared with the data collected for other Pb-BDC MOFs synthesized using harsh conditions (high temperatures). The equivalence between the reported diffractograms and the ones measured for Pb-BDC/H_2O and Pb-BDC/DMF reflects the success in our synthesis and the high crystallinity and quality of the resulting MOFs. The 3D structure of Pb-BDC/H_2O and Pb-BDC/DMF is also depicted

in Figure S1. Briefly, Pb-BDC/H_2O crystallizes in a very dense structure within the monoclinic space group *$P2_1/c$* and with the formula [Pb(BDC)(H_2O)], while Pb-BDC/DMF is a porous structure that crystallizes in a monoclinic system with C2/c space group with the formula [$Pb_3(BDC)_3(DMF)_{3.5}$], as previously reported [2, 3].

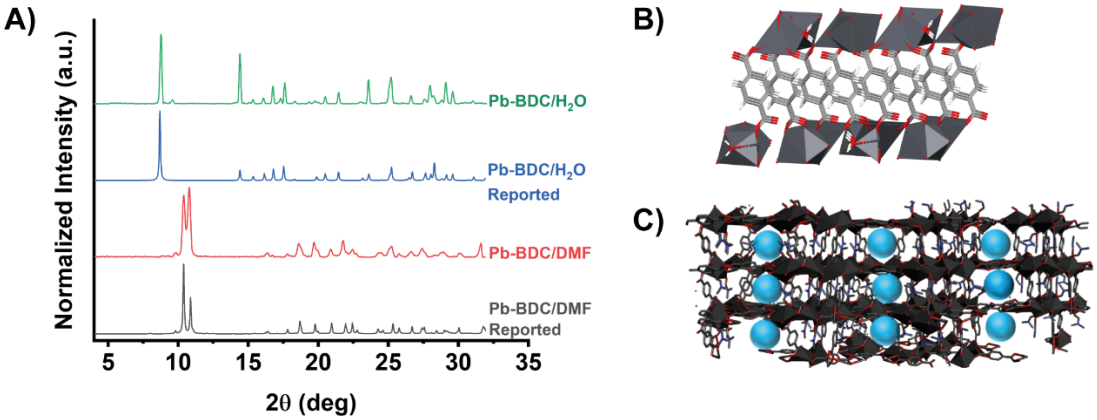

Figure S1. PXRD patterns of the Pb-BDC/H_2O and Pb-BDC/DMF MOFs previously reported, (CCDC 233113 and 662034, respectively) compared with the ones synthesized in this work. **B), C)** 3D structures of **B)** Pb-BDC/H_2O and **C)** Pb-BDC/DMF. The blue spheres denote the accessible nanopores that can accommodate the DMF molecules.

Morphological Characterization: The SEM and AFM micrographs of Pb-BDC/H_2O reveal that the crystals are in the form of nanosheets with a longitudinal size of 0.6-1 µm and a height of just 50-100 nm (Figure S2 A-D). On the other hand, the morphology of Pb-BDC/DMF crystals is columnar with a larger size (~2.5 µm) and height (~120 nm) as shown in Figure S2 E-H.

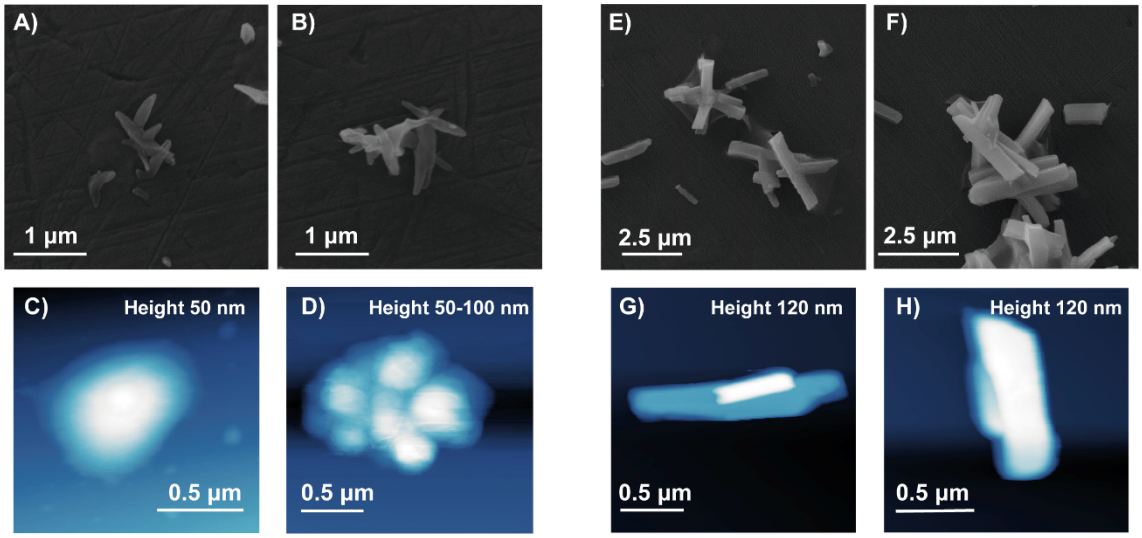

Figure S2. SEM micrographs of **A-B)** Pb-BDC/H_2O and **E-F)** Pb-BDC/DMF MOFs. AFM images of **C-D)** Pb-BDC/H_2O and **G-H)** Pb-BDC/DMF MOFs.

Chemical Characterization: The FTIR spectra of Pb-BDC/H_2O and Pb-BDC/DMF MOFs show no remarkable differences apart from the broad band at ~3050 cm^{-1} detected for Pb-BDC/H_2O, and those at ~2930 and ~1640 cm^{-1} observed for Pb-BDC/DMF (Figure S3). Those bands are clearly associated to the presence of water and DMF solvents. For instance the broad band at ~3050 cm^{-1} corresponds to the O-H stretch modes of water [4], and that at ~1640 cm^{-1} can be attributed to the υ(C = O) stretching mode of residual DMF molecules [5]. The FTIR spectra of both samples display vibrational bands at ~1540, 1360, 1300, 1150, 1090, 1010, 890, 820 and 740 cm^{-1} (Figure S3). Those are comparable to the bands previously described for the silver-based OX-2 MOFs [1]. Therefore, and following previous assignments, the bands at 1520 and 1360 cm^{-1} can be attributed to asymmetric and symmetric stretching modes of the carboxylic groups of the BDC linker coordinated to the Pb metal center, while the bands at the lowest frequencies are ascribable to different modes (υ(C = C) stretching mode, β(CCH) and γ(CCC) bending) of the BDC linkers [1].

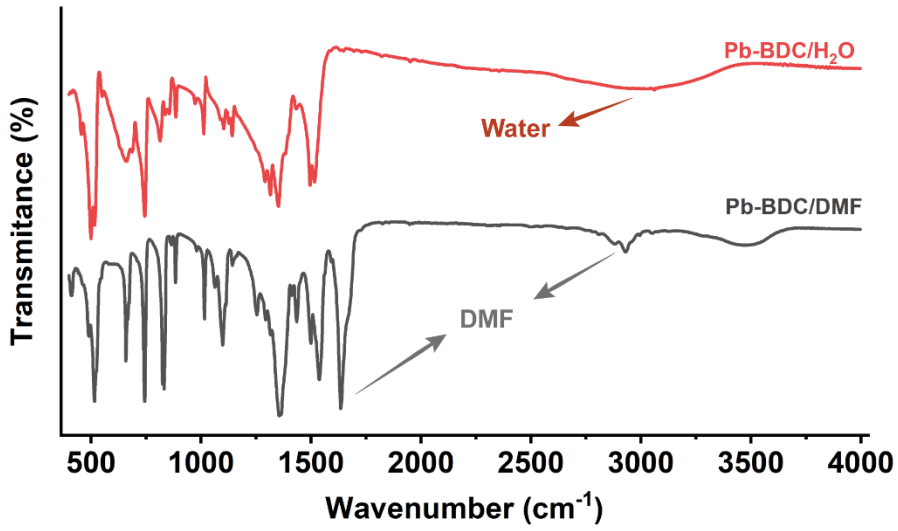

Figure S3. FTIR spectra of Pb-BDC/H_2O (red line) and Pb-BDC/DMF (grey line) MOFs.

Thermogravimetric Characterization: The thermal stability of both materials was characterized by thermogravimetric analysis (TGA) (Figure S4). Moreover, the chemical composition is also determined and compared with the theoretical values.

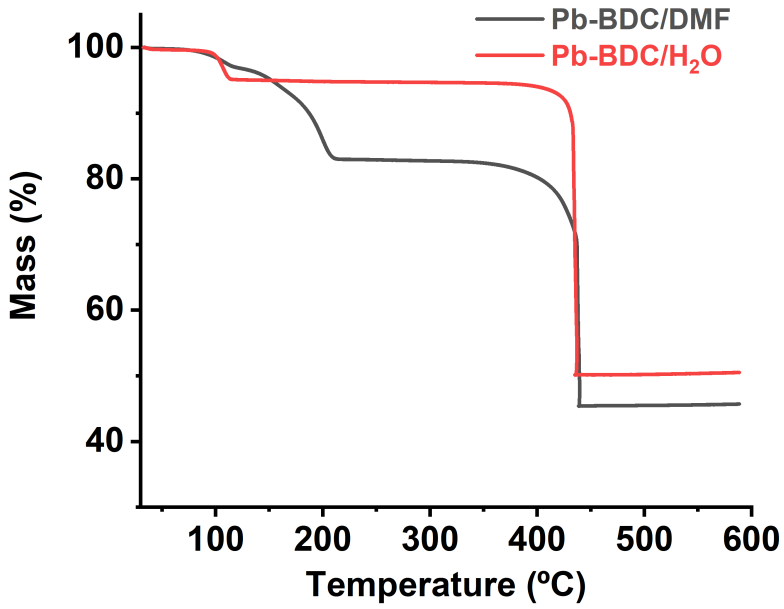

Figure S4. Thermogravimetric results obtained for Pb-BDC/H_2O (red line) and Pb-BDC/DMF (grey line) MOFs.

For the Pb-BDC/H_2O MOF there exists two clear steps, corresponding to the loss of water (100ºC, 5%) and the decomposition of the MOF (435ºC, 45%). Similarly, the Pb-BDC/DMF MOF shows a loss of DMF solvent (200ºC, 17%) and then another step which is the decomposition of the framework (435ºC, 38%). Considering that the decomposition of the MOFs corresponds to the weight of BDC linkers, and that the chemical formula of these MOFs is [Pb(BDC)(H_2O)] and [Pb_3(BDC)$_3$(DMF)$_{3.5}$], it is possible to estimate the chemical composition of our materials and compared it to the theoretical ones.

MOF formula	**% theoretical**	**% weight loss from TGA**
Pb(BDC)(H_2O) Mw = 389 g/mol	**Pb → 53%**	50 %
	BDC → 42%	45%
	H_2O → 5%	5%
Pb_3(BDC)$_3$(DMF)$_{3.5}$ Mw = 1368.5 g/mol	**Pb_3 → 45%**	45%
	BDC_3 → 36%	38%
	$DMF_{3.5}$ → 19%	17

4. Long-Lived Emission Time-Resolved Characterization

In this section, we present values of the long-lived emission decays of the Pb-BDC MOFs at 298 K together with their contribution to the signal. We also show the associated decay emission spectra of Pb-BDC/H_2O recorded at 77 K. Note that it was not possible to record any spectra for Pb-BDC/DMF, because at this low temperature there was a lack of long-lived component.

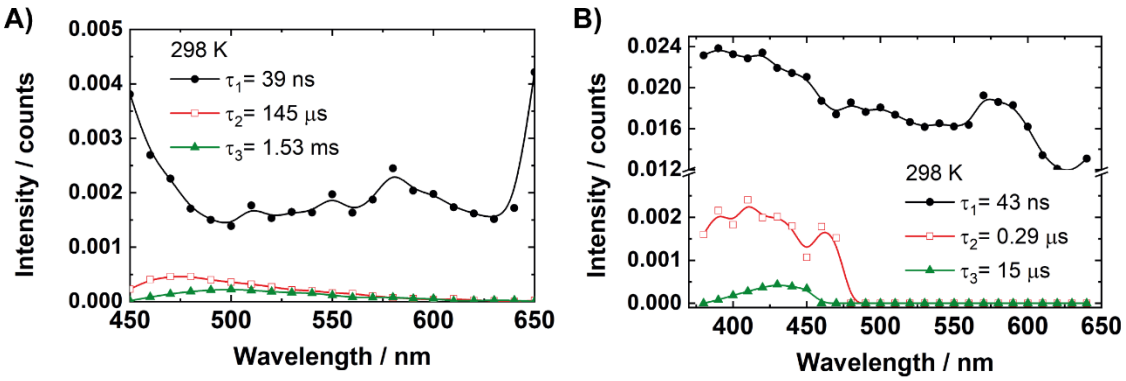

Figure S5. Representation of the emission lifetimes and contribution to the signal of **A)** Pb-BDC/H_2O and **B)** Pb-BDC/DMF MOFs.

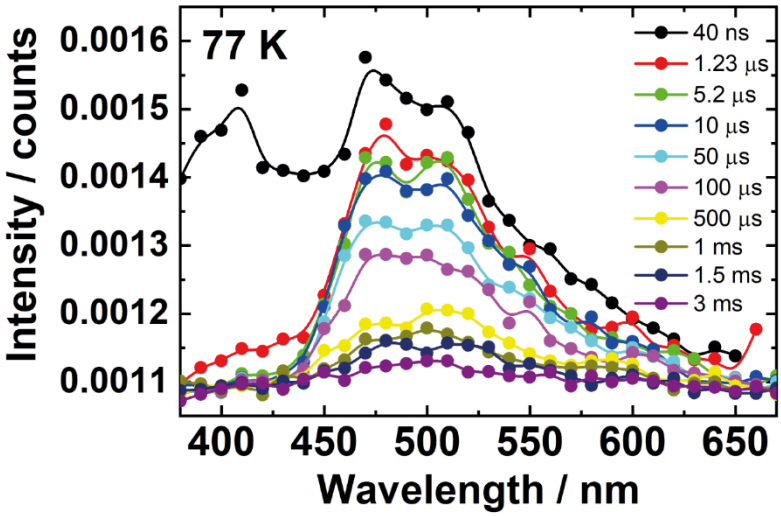

Figure S6. Decay associated emission spectra of Pb-BDC/H_2O collected at 77 K. The emission spectra were recorded at the times indicated in the inset.

4. Chemical Detection

In this subsection, the luminescent response of both Pb-BDC MOFs to the presence of different volatile organic compounds (VOCs) is tested. The experiments were performed by measuring a suspension of 4 mg of each MOF in 4 ml of the corresponding solvent. These suspensions were sonicated for 15 min to disperse the MOF. It is worth to note the full quenching of the emission of Pb-BDC/DMF MOF in the presence of acetone (Figure S6 D-E). Furthermore, we have tested the selectivity towards low levels of acetone of this MOF while immersed in DMF (Figure S7).

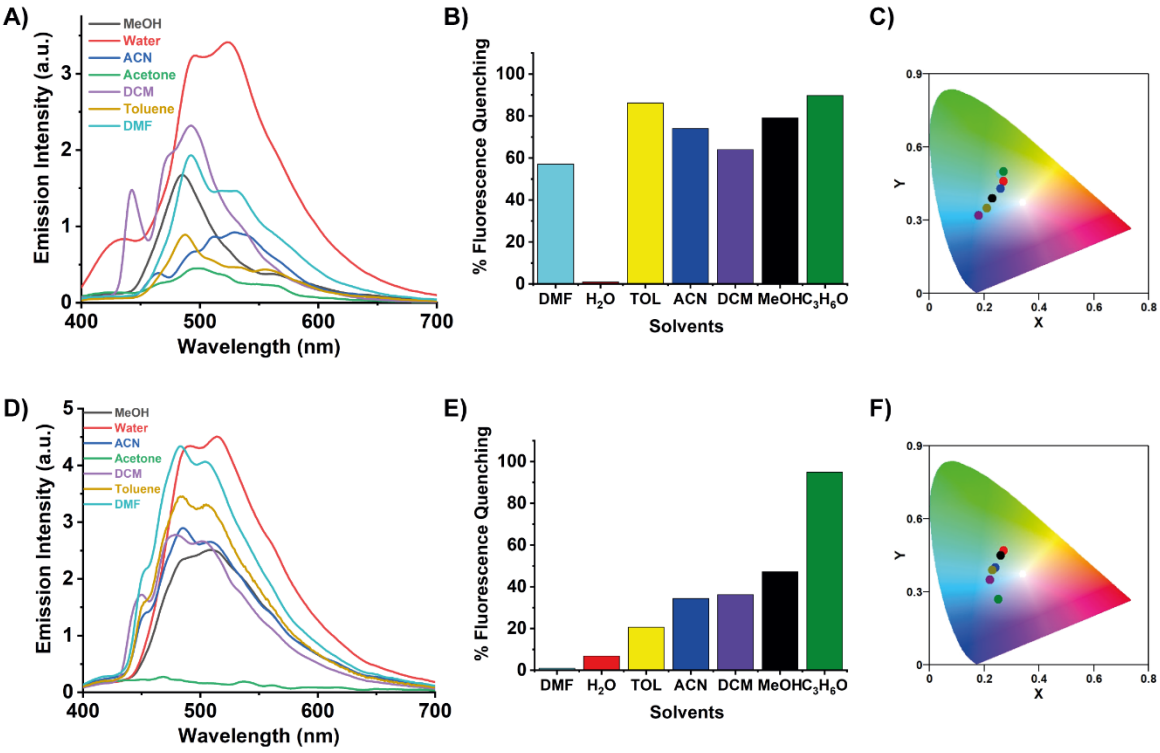

Figure S7. Emission spectra of **A)** Pb-BDC/H_2O and **D)** Pb-BDC/DMF MOFs immersed in different VOCs. **B), E)** Representation of the emission quenching of **B)** Pb-BDC/H_2O and **E)** Pb-BDC/DMF MOFs in the indicated solvents. **C), F)** CIE coordinates of the emission of **C)** Pb-BDC/H_2O and **F)** Pb-BDC/DMF MOFs in the different solvents. The colors match with those showed in figures B) and E), respectively.

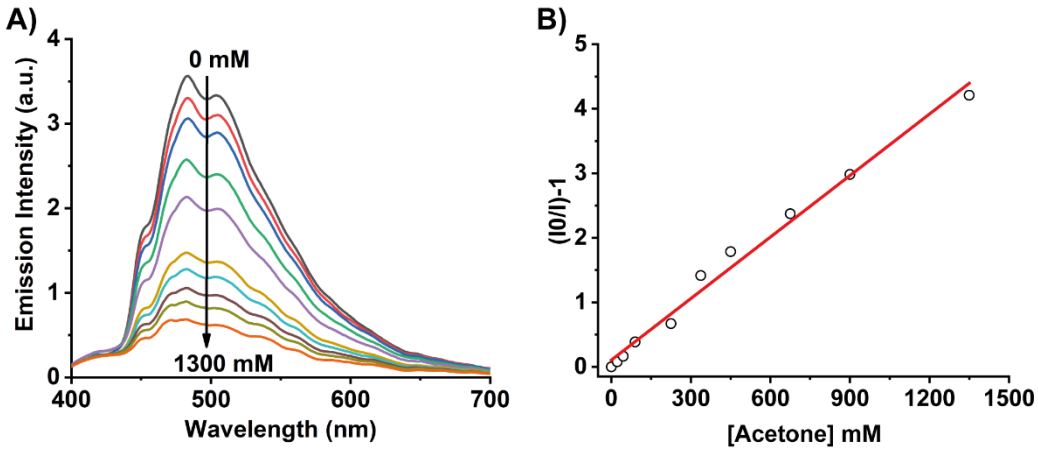

Figure S8. **A)** Emission spectra of Pb-BDC/DMF dispersed in DMF upon the addition of different amounts (expressed in mM) of acetone. **B)** Stern-Volmer analysis of the quenching of Pb-BDC/DMF by the addition of acetone.

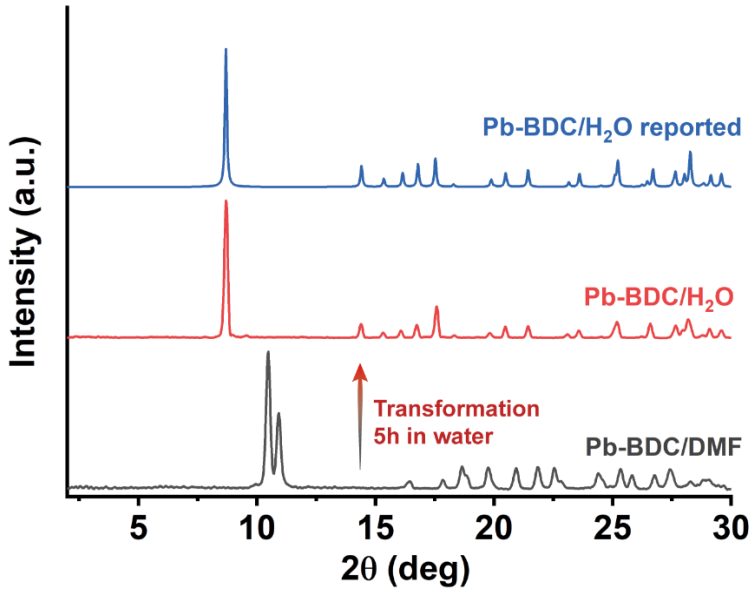

Figure S9. PXRD patterns of pristine Pb-BDC/DMF MOF and the powder obtaining by soaking the former in water for 5h. It is worth to note the equivalence of the diffraction peaks between the second structure and the reported structure of Pb-BDC/H_2O, indicating a solvent induced MOF-to-MOF transformation.

5. Thermochromism

In addition to the linear decrease of the emission intensity with increasing temperatures demonstrated by these two MOFs, both materials could be used as ratiometric sensors as shown in the following figures.

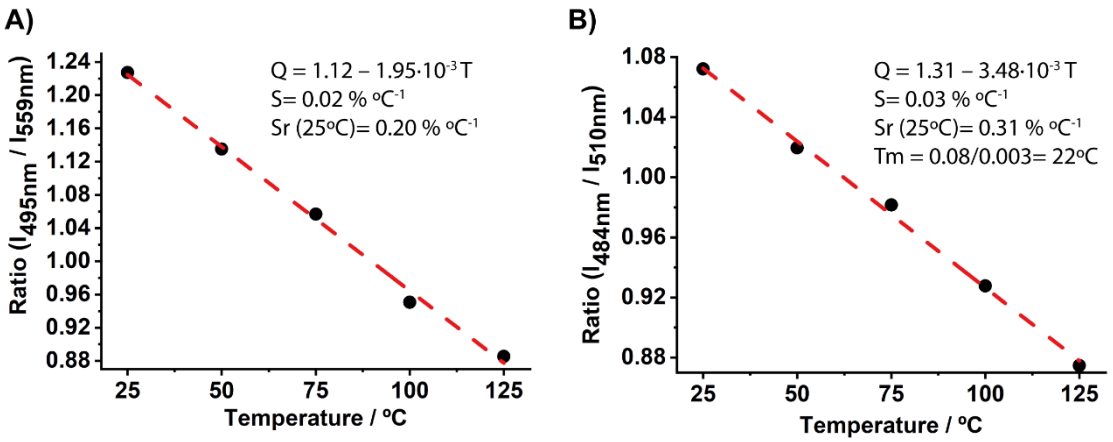

Figure S10. Representation of the linear ratiometric response of the emission of **A)** Pb-BDC/H_2O and **B)** Pb-BDC/DMF MOFs with increments in the temperature.

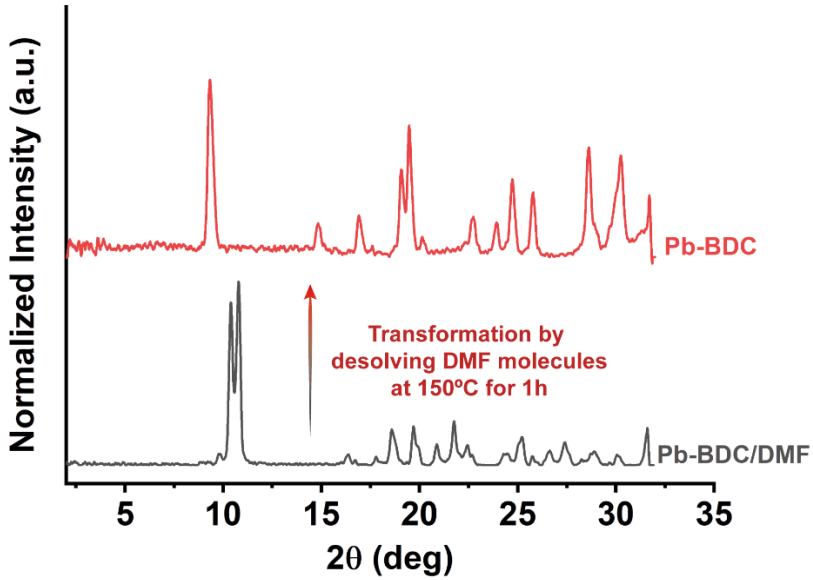

Figure S11. PXRD pattern of Pb-BDC/DMF and the material obtained upon heating the former at 150ºC for 1h. This procedure produces a structural change into a more packed arrangement [6].

6. LEDs

Herein, we show the deconvolution of the electroluminescence (EL) spectra of the MOF-LED devices using the RTP-MOFs as the EL layer. Additionally, the I-V curves of the devices when using different anodes and cathodes are also displayed.

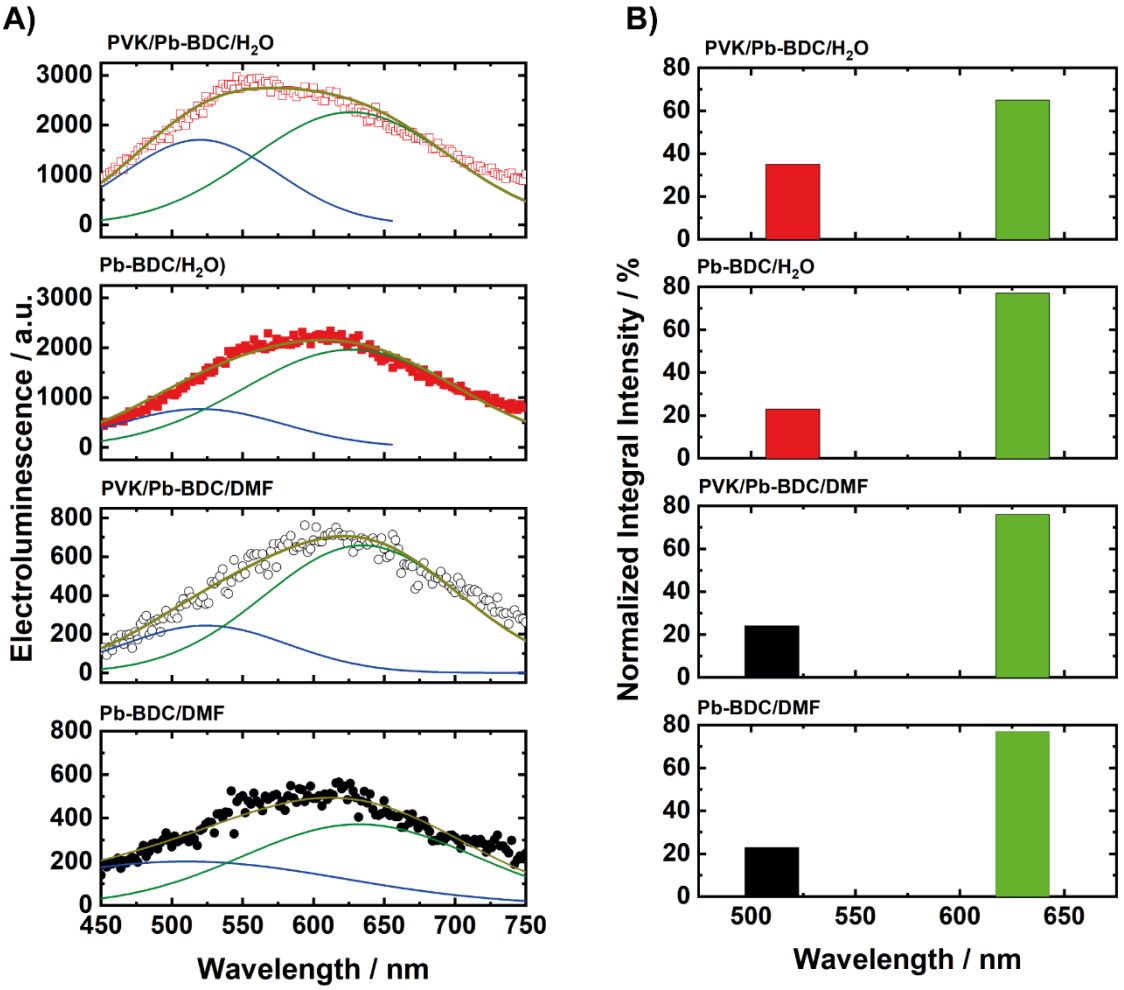

Figure S12. **A)** Deconvolution of the electroluminescence spectra of the different devices (indicated in each graph). **B)** Contribution of each of the bands obtained from the deconvolution of figure A.

The most plausible explanation about the 5 times higher intensity of the Pb-BDC/H_2O device is related to the MOF structure rather than the presence of defects. The denser structure of Pb-BDC/H_2O will favour the emissive triplet state generation and the charge mobility recombination processes. To validate that the denser packing structure boost not only the emissive triplet state generation but also enhance the charge mobility, single carrier devices were fabricated and characterized. For "hole only" devices an

ITO/PEDOT:PSS/ and Ag cathode were used, while, for the "electron only" device, an Yb anode and TPBi/Al cathode were employed. By doing this, the electron carrier and the hole carrier were blocked respectively because there is a huge mismatch between the work function of the electrodes and the electroluminescent materials. No emission from those devices was observed, and as it can be seen from Figure S12 a lower current density was obtained in comparison to the normal LEDs (Figure 4A). All together gives unequivocal evidence of only a single carrier is present in these devices. From those results several outcomes can be extracted: a) similar I-V curve for electron and hole carrier devices were observed for Pb-BDC/H_2O and b) smaller current density for hole carrier is observed in the Pb-BDC/DMF devices. Herein, better and more balanced carrier mobility is observed for Pb-BDC/H_2O device, where the hyperfine coupling is stronger.

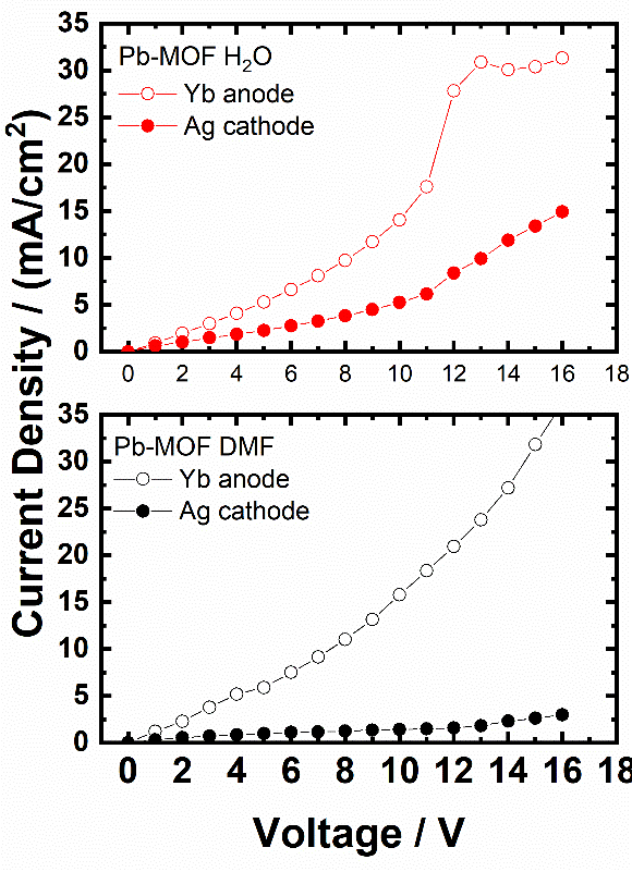

Figure S13. I-V curves of the different devices prepared using Yb and Ag as anode and cathode respectively.

References:

[1] Gutiérrez, M.; Martín, C.; Souza, B. E.; Van der Auweraer, M.; Hofkens, J.; Tan, J.-C., Highly luminescent silver-based MOFs: Scalable eco-friendly synthesis paving the way for photonics sensors and electroluminescent devices. *Appl. Mater. Today* 2020, *21*, 100817.

[2] Yang, J.; Ma, J.-F.; Liu, Y.-Y.; Ma, J.-C.; Batten, S. R., Organic-Acid Effect on the Structures of a Series of Lead(II) Complexes. *Inorg. Chem.* 2007, *46* (16), 6542-6555.

[3] Dale, S. H.; Elsegood, M. R. J.; Kainth, S., Poly[lead(II)-[mu]2-aqua-[mu]4-terephthalato]. *Acta Crystallographica Section C* 2004, *60* (2), m76-m78.

[4] Choi, J.-H.; Cho, M., Computational IR spectroscopy of water: OH stretch frequencies, transition dipoles, and intermolecular vibrational coupling constants. *J. Phys. Chem.* 2013, *138* (17), 174108.

[5] Ren, Y.-K.; Liu, S.-D.; Duan, B.; Xu, Y.-F.; Li, Z.-Q.; Huang, Y.; Hu, L.-H.; Zhu, J.; Dai, S.-Y., Controllable intermediates by molecular self-assembly for optimizing the fabrication of large-grain perovskite films via one-step spin-coating. *J. Alloys Compd.* 2017, *705*, 205-210.

[6] Li, Z.-P.; Xing, Y.-H.; Wang, C.-G.; Li, J.; Zeng, X.-Q.; Ge, M.-F.; Niu, S.-Y., A New Coordination Polymer [Pb(1,4-BDC)]n Containing a Unique μ6-Bridging Coordination Mode. 2009, *635* (11), 1650-1653.